Estimation and Uncertainty Quantification of Magma Interaction Times using Statistical Emulation

Luca Insolia[1], Stéphane Guerrier[1,2], Chiara P. Montagna[3],
Maria-Pia Victoria-Feser[1] & Luca Caricchi[4]

[1] Geneva School of Economics and Management, University of Geneva, Switzerland; [2] Faculty of Science, University of Geneva, Switzerland; [3] Istituto Nazionale di Geofisica e Vulcanologia, Sezione di Pisa, Italy; [4] Department of Earth Sciences, University of Geneva, Switzerland.

Abstract

Evolution of volcanic plumbing systems towards eruptions of different styles and sizes largely depends on processes at crustal depths that are outside our observational capabilities. These processes can be modeled and the outputs of the simulations can be compared with the chemistry of the erupted products, geophysical and geodetic data to retrieve information on the architecture of the plumbing system and the processes leading to eruption. The interaction between magmas with different physical and chemical properties often precedes volcanic eruptions. Thus, sophisticated numerical models have been developed that describe in detail the dynamics of interacting magmas, specifically aimed at evaluating pre-eruptive magma mingling and mixing timescales. However, our ability to explore the parameters space in order to match petrological and geophysical observations is limited by the extremely high computational costs of these multiphase, multicomponent computational fluid dynamics simulations.

To overcome these limitations, we present a statistical emulator that is able to reproduce the numerical simulations results providing the temporal evolution of the distribution of magma chemistry as a function of a set of input parameters such as magma densities and reservoir shapes. The whole rock composition of volcanic rocks is one of the most common measurable parameter collected for eruptions. The statistical emulator can be used to invert the observed distribution of whole rock chemistry to determine the duration of interaction between magmas preceding an eruption and identify the best matching input paramaters of the numerical model. Importantly, the statistical emulator intrinsically includes error propagation, thus providing confidence intervals on predicted interaction timescales on the base of the intrinsic uncertainty of the input parameters of the numerical simulations.

Keywords: Volcanology, Petrology, Magma Dynamics, Statistical Emulation

1. Introduction

Magmatic processes preceding volcanic eruptions occur at depths of few to tens of kilometers and are therefore not directly accessible: the only direct information about pre-eruptive magma storage conditions is provided by the volcanic rock record. Thus, textural (Cashman, Marsh, 1988; Higgins, 2000; Zellmer et al., 2020), rheological (Heap et al., 2020; Hess, Dingwell, 1996; Lavallée et al., 2007; Lejeune, Richet, 1995; Pistone et al., 2012) and chemical (Marsh, 1981; Maclennan, 2019; Zellmer et al., 2020; Neave et al., 2014; Putirka, 2008a; Edmonds et al., 2019; Cassidy et al., 2016; Edmonds et al., 2010; Stock et al., 2018; Humphreys et al., 2012; Cooper, Kent, 2014; Davidson et al., 2007; Blundy,

Cashman, 2001) characterisation of volcanic rocks is central to our understanding of the processes leading to volcanic eruptions. However, to retrieve quantitative information on pre-eruptive processes from the analysis of the rock record, it is fundamental first to compare the chemistry of minerals, rocks and glasses with those produced experimentally (Nimis, 1995; Petrelli et al., 2020a; Putirka, 2008b) and then to compare the analyses with the results of experiments or numerical modelling (e.g., Caricchi et al., 2014; Annen et al., 2006; Jackson et al., 2018; Perugini et al., 2015). We will focus here on the comparison between volcanic rock record and numerical modelling results.

Physical modeling is a fundamental tool to link observable quantities at the Earth surface and magmatic processes at depth (e.g., Bagagli et al., 2017; La Spina et al., 2022). Modeling efforts have been directed both at tackling the complex thermochemistry of multiphase magmas (e.g., Gualda et al., 2012; Bohrson et al., 2014; Rummel et al., 2020; Keller, Suckale, 2019), in order to be able to replicate observed geochemical patterns in erupted products (crystals, melt inclusions, e.g., Caricchi et al. 2018; Wei et al. 2022) as well as emitted gas chemistry and fluxes (e.g., Chiodini et al., 2012), and at replicating observed geophysical signals such as ground deformation, gravity anomaly and seismicity recorded at active volcanoes (e.g., Poland, Dalfsen de Zeeuw-van, 2021; Matoza, Roman, 2022). Inclusion of all relevant physics is often impossible, given the wide variety of length and time scales that characterize volcanic systems at large; therefore, different approximations are typically used to target specific questions: homogeneous reservoirs are often assumed in order to model ground deformation (e.g., Mogi, 1958; Zhong et al., 2019); magma motion is usually neglected when modeling crystal growth patterns (e.g., Iovine et al., 2017; Petrone et al., 2018). Necessity of simplifying assumptions is also motivated by the very high computational costs of running large-scale, detailed simulations of the overall magmatic system evolution (Garg, Papale, 2022). This also largely limits our ability to explore the wide range of initial conditions and input parameters that characterize magmatic systems, such as temperature and pressures/depth of melt reservoirs, as well as their size and shape and melt chemistry and volatiles content. Moreover, as properties of magma reservoirs at depth cannot be measured, models' initial conditions are typically characterized by large uncertainties, which are, in turn, difficult to define.

Because of the required assumptions and uncertainties even on the range of some of the input parameters of physical models, it is often impossible to quantitatively assess the impact of initial assumptions in the final results of the models. This would require the realisation of millions of simulations to systematically investigate the full range of input parameters. Additionally, the use of complex physical models during volcanic unrest can be unpractical as the realisation of simulations can be long and the integration of continuous streams of data not straightforward (Selva et al., 2012).

This is where the combination of physical modelling and statistical emulation becomes essential. Using the outputs of simulated physical states and the corresponding values for the theoretical parameters – i.e., simulated data produced by a simulator given a set of input parameters – a statistical emulator allows one to predict the physical model output given a specific input, along with an associated measure of the uncertainty on this prediction. More precisely, a statistical emulator is a probabilistic model that links (summary statistics computed from) simulated data, produced by a theoretical physical model (i.e., the simulator), to the parameters' values used to produce the simulation results. Once trained on a series of simulated data, the statistical emulator can be used on observed data to calibrate the possible values of some of the input parameters of the underlying physical process. Statistical emulation is a very

popular method in environmental sciences. Sacks et al. (1989); Currin et al. (1991); Higdon et al. (2008); Kennedy, O'Hagan (2001); Santner et al. (2003) use a Gaussian process to model the uncertainty; due to the long computational times and large number of required emulators, in practice a (multivariate) regression model is often preferred (see e.g., Salter, Williamson 2016 for a discussion and references). Notably, different statistical emulators that rely on various statistical assumptions are regularly proposed, and they depend both on the physical model and the available data; see e.g., Mahmood et al. (2015); Yang et al. (2020); Guillas et al. (2018) to cite just a few.

In this paper we present results from a numerical model of magma mingling, tailored for the Campi Flegrei magmatic system (Montagna et al., 2022). We show how silicate melt composition evolves as two parental magmas interact in a relatively shallow reservoir at 3 km depth, approaching compositional homogeneity (Montagna, Papale, 2018), for different setups characterized by varying reservoir shape and magmatic volatile contents. A statistical emulator is then trained on these results; we present the high accuracy it achieves in reproducing simulated results, even at large down-sampling, and the error quantification associated with this method.

2. Magma dynamics models

The very existence of magma within the Earth's crust requires prolonged input of mass and energy (i.e., heat) from the mantle source (Glazner et al., 2004; Annen et al., 2006; Karakas et al., 2017). Thus, the progressive assembly of volcanic plumbing systems naturally results in the interaction between resident, and generally colder, magma and hot, generally more primitive magma rising through the crust. Abundant field evidence exists for this process, both in the plutonic and volcanic rock record (Blundy, Sparks, 1992; Perugini, Poli, 2005; Ridolfi et al., 2015; Morgavi et al., 2016, 2017), and in some cases such interaction can culminate in a volcanic eruption (Caricchi et al., 2021). Examples of magma input triggering volcanic activity can be identified at Campi Flegrei, Santorini, Yellowstone, and Long Valley (Wark et al., 2007; Druitt et al., 2012; Morgavi et al., 2016; Forni et al., 2018), and approaches have been proposed to determine the duration of magma interaction preceding an eruption (Perugini et al., 2015). Here, we simulate the dynamical evolution of a melt-dominated magmatic reservoir subject to the injection of deeply-sourced, more primitive, volatile-richer (buoyant) magma (Montagna et al., 2015, 2022), focusing on the quantification of the time scales of magmatic convection and mingling.

2.1. Physical model setup

Numerical simulations of magma chamber replenishment were performed using the finite-element C++ code GALES (Longo et al., 2012a; Garg et al., 2018a,b). The physico-mathematical model describes the space-time dynamics of a multicomponent mixture consisting of silicate melt in thermodynamical equilibrium with a gas phase at the local conditions of pressure, temperature and composition (Longo et al., 2012b; Papale et al., 2017; Bagagli et al., 2017; Garg et al., 2019). The conservation equations for the mass of single components and momentum of the whole mixture are solved together with the gas-liquid thermodynamic equilibrium model (Papale et al., 2006) and the constitutive equations for multiphase, multicomponent mixture properties density and viscosity (Reid et al., 1977; Ishii, Zuber, 1979; Lange, 1997; Giordano et al., 2008).

We explore buoyant magma mixing and its timescales based on the archetypal case of the Campi Flegrei volcanic system, where occurrences of interacting magmas have been widely testified (Tonarini et al., 2009; Arienzo et al., 2010; Fourmentraux et al., 2012; Forni et al., 2018). We model the injection of CO_2-rich, shoshonitic magma coming from a deep reservoir into a shallower, much smaller one, containing more evolved and partially degassed phonolitic magma (Mangiacapra et al., 2008; Arienzo et al., 2009; Di Renzo et al., 2011).

Different geometries and volatile contents of the shallow chamber were considered to account for a range of possible conditions at Campi Flegrei. Figure 1 shows the simulated domain and summarizes the conditions for the numerical simulations; the deep chamber contains a shoshonitic magma with 2 wt% H_2O and 1 wt% CO_2.
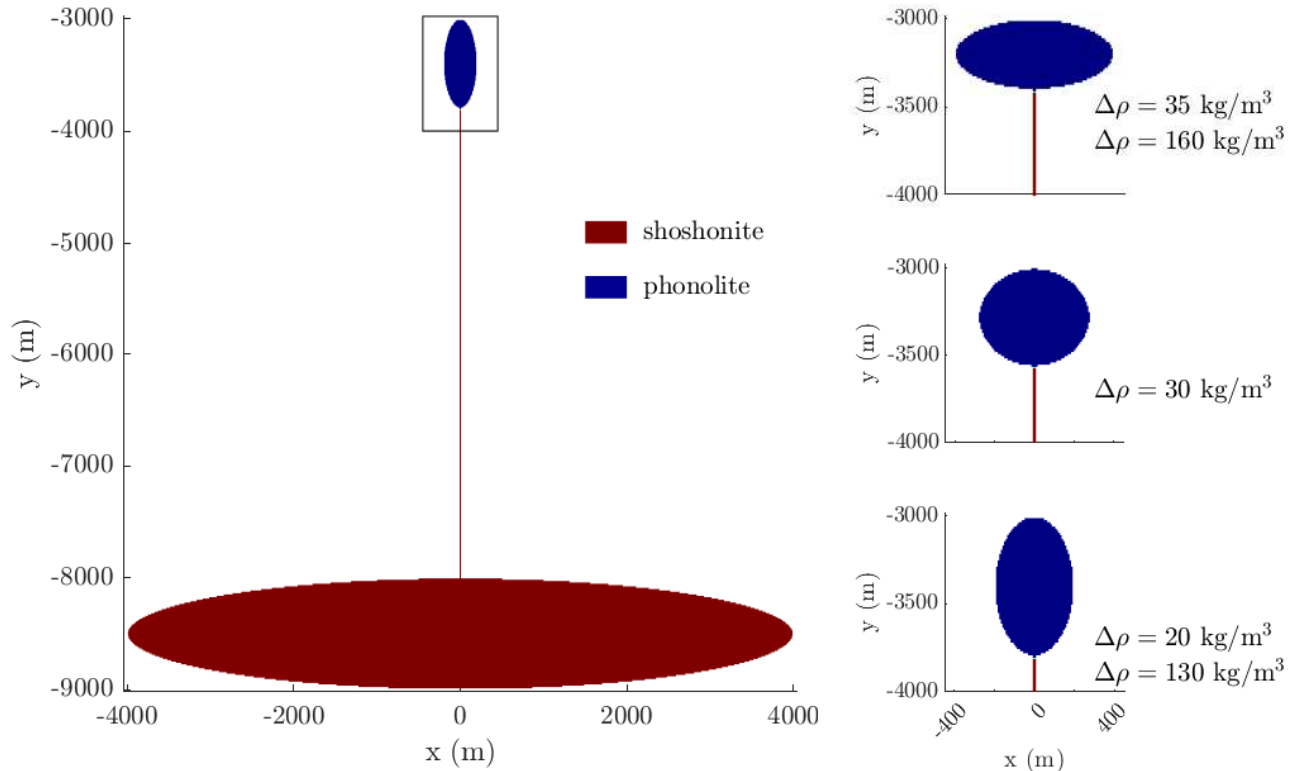
Figure 1. Summary of the five simulated settings. The upper chamber is either elliptical, with semi-axes of 200 m and 400 m, or circular, with radius of 283 m to keep the same surface area. The dyke, which at time 0 hosts shoshonite like the deep chamber, is 20 m wide. The deep reservoir is elliptical, with semi-axes of 8 km and 1 km.

The different settings in Figure 1 can be represented by two meaningful quantities, the initial density difference at the interface among the two end-member magmas (shallow phonolite and deep shoshonite) $\Delta\rho$, and the aspect ratio of the shallow reservoir a. Table 1 shows the values of these parameters for the five simulated scenarios.

2.2. MAGMA MINGLING

As the two magmas come into contact at time 0, a gravitational Rayleigh-Taylor instability (Chandrasekhar, 2013) develops at the interface because of the the density difference $\Delta\rho$ between the denser magma in the shallow reservoir and the volatile-rich and less dense injected magma. Figure 2 shows the space-time evolution of the composition within

Table 1. Values of the input parameters for each simulated scenario.

	aspect ratio a	density difference $\Delta\rho$, $\mathrm{kg\,m^{-3}}$
simulation 1	0.5	35
simulation 2	1.0	30
simulation 3	2.0	20
simulation 4	0.5	160
simulation 5	2.0	130

the shallower, initially phonolitic reservoir where shoshonitic magma is injected.
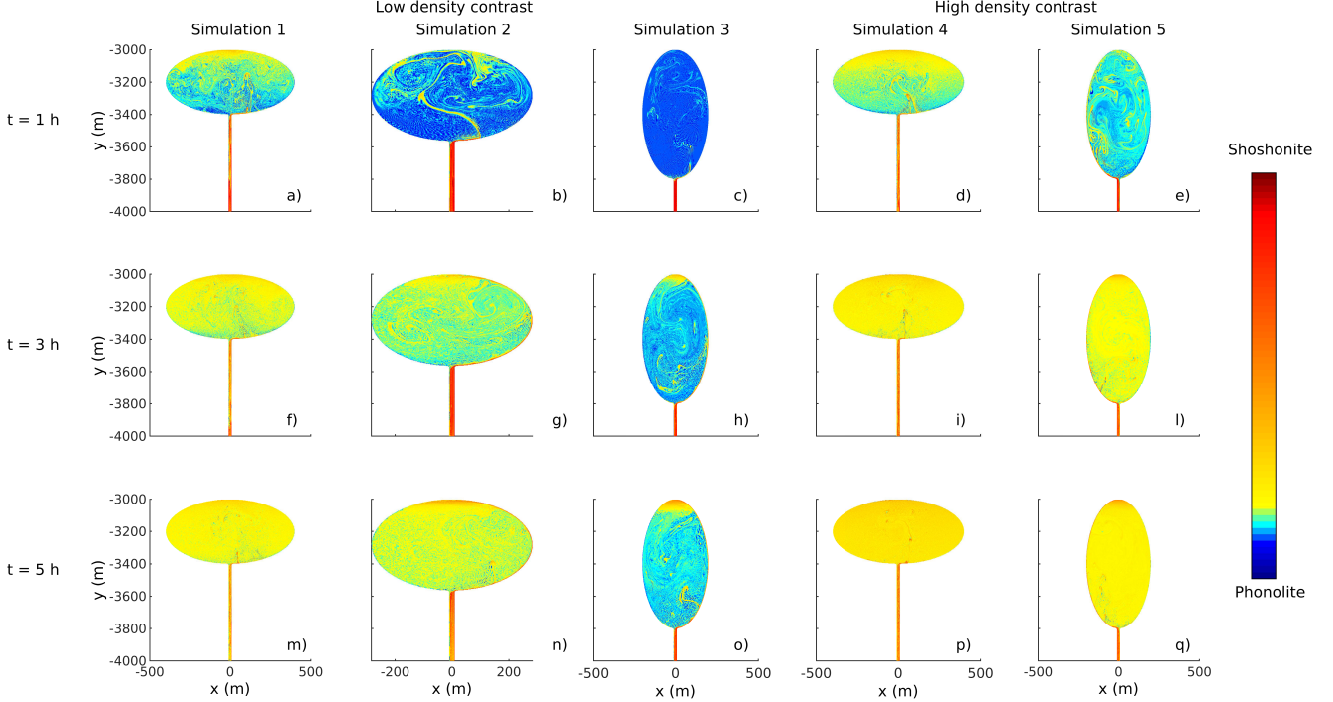
Figure 2. Space-time evolution of composition in the upper region of the simulated domain, for the different scenarios. Rows represent different times, columns represent different simulations.

Plumes of light magma rise into the shallow reservoir and trigger convective patterns enhancing magma mixing, while a portion of the degassed phonolitic magma initially hosted in the shallow reservoir sinks through the feeding dyke. With time a density-stratified magma chamber develops (Figure 2). The space-time evolution of composition within the reservoir depends both on its aspect ratio and on the initial density contrast (Figure 2), but in all cases it testifies for the progressive homogenisation of magma chemistry (Montagna et al., 2015).

During the magmatic interaction described above, an eruption can occur, sampling the magma from the reservoir. Here we assess the capacity of the distribution of erupted magma chemistry to return information on the duration of interaction preceding the eruption. This sort of information is essential to determine, from the study of past eruptions triggered by the interaction between magmas, the amount of time available between potential monitoring signs of magma input into a relatively shallow reservoir and eruption (Bagagli et al., 2017). Instead of performing a large number of numerical simulation, we resort to statistical emulation. We use the distribution of magma chemistry as

function of time obtained from the numerical simulations to calibrate the statistical emulator. The final target of this approach is to build a model which, on the basis of the distribution of erupted magma chemistry, provides the timescales of magmatic interaction that preceded the eruption, and the associated uncertainties.

3. A Statistical Emulator

A statistical emulator (SE) is a probabilistic model that links summary statistics ($\mathbf{y} \in \mathcal{Y} \subseteq \mathbb{R}^J$) computed from simulated information, produced by a theoretical (complex) model (simulator), to the parameters' values ($\mathbf{x} \in \mathcal{X} \subseteq \mathbb{R}^K$) used to produce the simulation results. Very generally, one considers theoretical models that are complex enough so that simulating one possible outcome, i.e., the outcome obtained with one (set of) value for the parameters governing the theoretical model (i.e., $\mathbf{x}_i \in \mathcal{X} \subseteq \mathbb{R}^K$), is computationally very demanding. In these cases, the simulator cannot simulate information for all sets of possible parameters $\mathbf{x}_i$, but instead can simulate from a finite sample, say $\mathbf{x}_i$ for $i = 1, \ldots, m$, of carefully chosen combinations of values for the $\mathbf{x}_i$'s. In the context of time dependent outputs, in full generality, a SE postulates a relationship of the form

$$y_{itj} = f_j(\mathbf{x}_{it}, \boldsymbol{\theta}) + \varepsilon_{itj}, \tag{1}$$

where $t = t_1, \ldots, t_{n_i}$ are the time points associated to the set of parameters $\mathbf{x}_i$, and $j = 1, \ldots, J$ indexes summary statistics. Thus, in vector form, we have

$$\mathbf{y}_i = \boldsymbol{f}(\mathbf{x}_i, \boldsymbol{\theta}) + \boldsymbol{\varepsilon}_i = \left[f_1(\mathbf{x}_{it_1}, \boldsymbol{\theta}), \ldots, f_1(\mathbf{x}_{it_{n_i}}, \boldsymbol{\theta}), \ldots, f_J(\mathbf{x}_{it_1}, \boldsymbol{\theta}), \ldots, f_J(\mathbf{x}_{it_{n_i}}, \boldsymbol{\theta}) \right]^T + \boldsymbol{\varepsilon}_i. \tag{2}$$

Indeed, the outcomes are obtained at different n_i time points and, for each of these times points (and other associated simulation parameters), J summary statistics can be computed. One also supposes, very generally, that $\boldsymbol{\varepsilon}_i \sim (\mathbf{0}, \boldsymbol{\Sigma})$, where $\Sigma_{kl} = \sigma_k^2$ for $k = l$ and $k, l = 1, \ldots, J \cdot n_i$. The vector of parameters $\boldsymbol{\theta} \in \boldsymbol{\Theta} \subseteq \mathbb{R}^p$ is unknown, and needs to be estimated, given a series $\mathbf{y}_i$ of size m (simulations) of J summary statistics, computed at n_i time points, that are extracted from the outcomes produced by the simulator using a series of (size m of) K parameters' values $\mathbf{x}_{it}$ governing the simulator. The noise $\boldsymbol{\varepsilon}_i$ captures the approximation error of the link functions f_j in (2), which can be made as complex as possible, but will never match exactly the true underlying theoretical process. The noise is random, and we suppose that its (probability) distribution is fully specified by its first two moments – i.e., for the i-th simulation, $\mathbb{E}[\boldsymbol{\varepsilon}_i] = \mathbf{0}$ and $\text{cov}(\boldsymbol{\varepsilon}_i) = \boldsymbol{\Sigma}$. Importantly, the components of $\boldsymbol{\Sigma}$ can be estimated to obtain an estimated covariance matrix $\hat{\boldsymbol{\Sigma}}$, which can be used to compute confidence intervals for the predictions provided by the SE.

3.1. Application to magma dynamics

We consider here a SE for the magma dynamics model presented in Section 2. The salient features of the SE, as well as the construction of its inputs, are highlighted in the flow chart of Figure 3. The input parameters $\mathbf{x}_{it}$, for the $m = 5$ simulations described in Table 1, are the aspect ratio of the shallow reservoir a_i, the initial density difference between the two end-member magmas $\Delta\rho_i$, and the interaction time $t = t_{k_i}$ (where $k_i \in \{1, \ldots, n_i\}$), so that $\mathbf{x}_{it} = [a_i, \Delta\rho_i, t_{k_i}]^T$. The output from the simulator is $\mathbf{D}_i$, an $r_i \times n_i$ matrix containing the silicate melt compositions
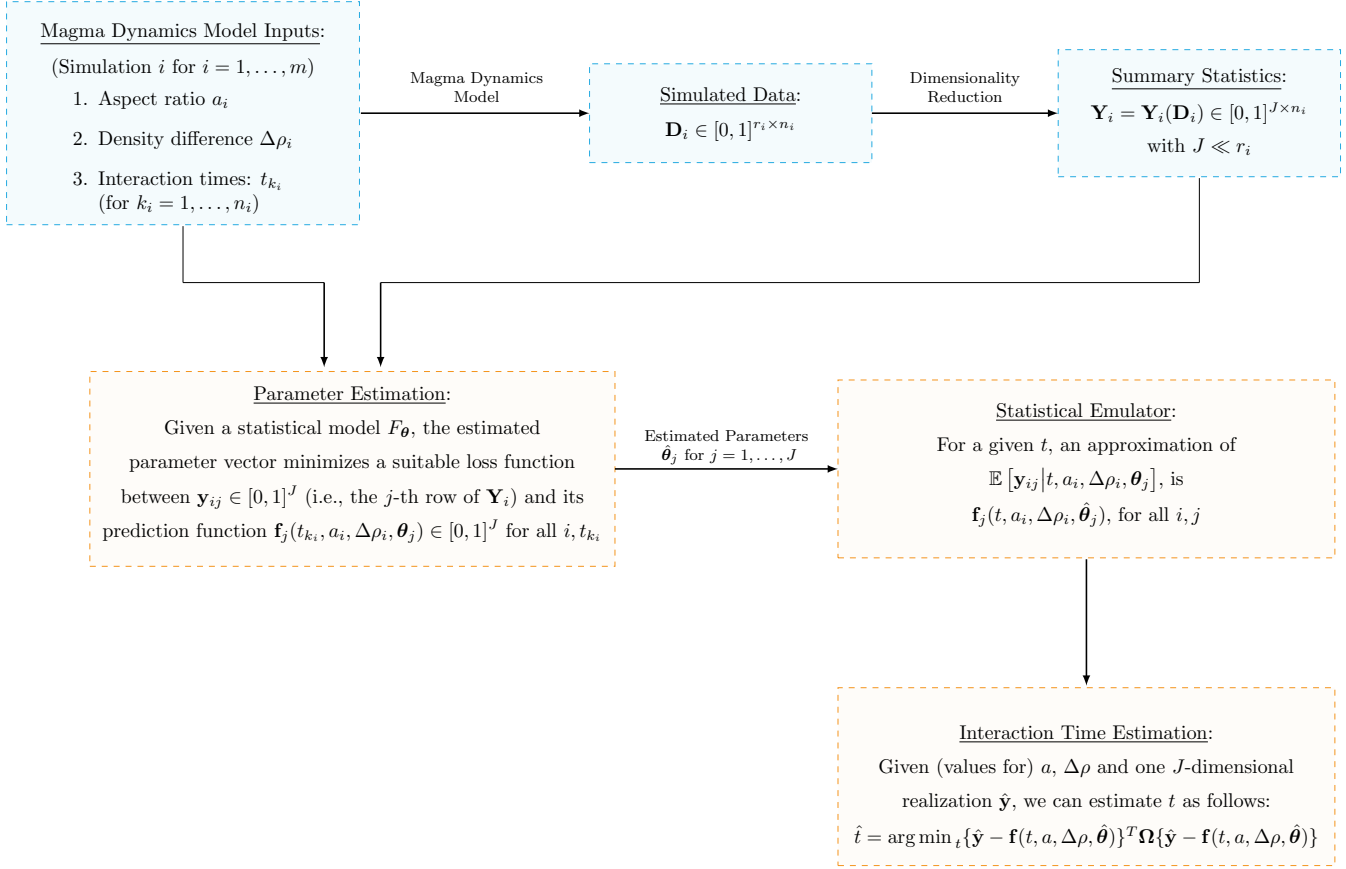
Figure 3. Flow chart from the simulator output to the statistical simulator and the prediction computation for the magma dynamics model in Section 2.

expressed as the proportions of the two end-member magmas, which are measured across r_i locations of the shallow reservoir at n_i interaction times. From this simulator output, summary statistics are computed to reduce the output dimension, and we have chosen to consider $J = 5$ quantiles (namely, 0.05, 0.25, 0.50, 0.75, and 0.95) computed from the distribution of the compositions over the r_i locations, with $J \ll r_i$. Namely, y_{itj} in (1) corresponds to the j-th row (i.e., j-th quantile) and t-th column of $\mathbf{Y}_i$ in Figure 3. The choice of these summary statistics is arbitrary and other summary statistics could be considered. Nevertheless, the SE provides satisfactory results with this choice (see Section 3.2). A statistical model as in (1) is then fitted to the summary statistics to obtain an estimated value $\hat{\boldsymbol{\theta}}$. The statistical model we consider is (1) with

$$
\begin{aligned}
f_j(t, \Delta\rho_i, a_i, \boldsymbol{\theta}_j) =& \beta_{1j} + \beta_{2j}t + \beta_{3j}\Delta\rho_i + \beta_{4j}a_i + \beta_{5j}t\Delta\rho_i + \beta_{6j}ta_i + \beta_{7j}\Delta\rho_i a_i + \beta_{8j}t\Delta\rho_i a_i + \beta_{9j}t^2 a_i \\
&+ \beta_{10j}t^3 a_i + \beta_{11j}t^4 a_i + \beta_{12j}t^2\Delta\rho_i a_i + \beta_{13j}t^3\Delta\rho_i a_i + \beta_{14j}t^4\Delta\rho_i a_i.
\end{aligned}
\tag{3}
$$

Therefore, the (unknown) parameters' vector $\boldsymbol{\theta} = \left[\boldsymbol{\theta}_1^T, \ldots, \boldsymbol{\theta}_J^T\right]^T$, with $\boldsymbol{\theta}_j = [\beta_{1j}, \ldots, \beta_{14j}, \sigma_j^2]^T$, has dimension $15 \cdot J = 75$. Again, the choice for the statistical model is arbitrary, but was selected as it provided satisfactory results for our case study (see Section 3.2). Then, through a suitable estimator of $\boldsymbol{\theta}_j$, say $\hat{\boldsymbol{\theta}}_j$, the (unknown) conditional expectation $\mathbb{E}[\mathbf{y}_{ij} | t, a_i, \Delta\rho_i, \boldsymbol{\theta}_j] = f_j(t, \Delta\rho_i, a_i, \boldsymbol{\theta}_j)$ can be estimated by $f_j(t, \Delta\rho_i, a_i, \hat{\boldsymbol{\theta}}_j)$. The latter can be used to predict t, or

indeed also a or $\Delta\rho$, given a set of outcomes $\mathbf{y} = [y_1, \ldots, y_J]^T$, which are usually obtained by field measurements. In our case the measurements are the whole rock chemistry of erupted volcanic rocks. Thus, given an observed $\hat{\mathbf{y}}$ (field measurements of whole rock chemistry of erupted rocks), and as precise as possible information about a (from geophysics) and $\Delta\rho$ (which can be calculated from the chemistry of the two end member magmas and existing models, see e.g., Lange 1997), a statistical emulation prediction for the interaction time t can be obtained through

$$\hat{t} = \arg\min_t \{\hat{\mathbf{y}} - \mathbf{f}(t, a, \Delta\rho, \hat{\boldsymbol{\theta}})\}^T \boldsymbol{\Omega} \{\hat{\mathbf{y}} - \mathbf{f}(t, a, \Delta\rho, \hat{\boldsymbol{\theta}})\}, \tag{4}$$

where $\boldsymbol{\Omega}$ is a suitably chosen positive definite weighting matrix. In our case study we simply choose $\boldsymbol{\Omega} = \boldsymbol{I}_5$ (i.e., the identity matrix of size $J = 5$). The prediction $\hat{t}$ defined in (4) is a classical minimum distance estimator with well-known statistical properties (see e.g., Newey, McFadden 1994). Namely, under plausible conditions, this estimator is consistent for t and asymptotically normally distributed, which implies that we can use this property to associate prediction errors when assessing error propagation (see Section 4).

3.2. PREDICTION ACCURACY

To evaluate the prediction accuracy of the SE, we consider, for the $\hat{\mathbf{y}}$, the ones directly obtained from the simulator, i.e., the *true* ones, for which a, $\Delta\rho$ and t are known. Then, we can compare the predicted interaction time $\hat{t}$ based on (4) to the known interaction time t, say the *true* interaction time, hence providing a way to evaluate the (in sample) prediction accuracy. Importantly, the following results are restricted to a random sub-sample encompassing 30% of the simulated interaction times t_{k_i}. This essentially allows us to reduce the computational burden. Finally, to estimate the parameters in (3), namely $\hat{\boldsymbol{\theta}}_j = [\hat{\beta}_{1j}, \ldots, \hat{\beta}_{14j}, \hat{\sigma}_j^2]^T$, we considered the Ordinary Least Squares (OLS) estimator for a standard linear regression model.

Panel (a) of Figure 4 compares predicted ($\hat{t}$) versus the true (t) interaction time (both measured in hours) for simulations 2-4 of Table 1. The resulting predictions across different simulation settings are very close to the true ones, which are represented by a dashed black line. This is further highlighted in panel (b) of Figure 4 which reports the associated absolute prediction errors, i.e., $|\hat{t} - t|$. Overall, absolute errors are lower than 0.8 hours across all settings and typically lower than 0.2 hours. However, a noticeable increase in prediction errors is present only for simulation 3 as interaction time approaches 5 hours. This might be due to the fact that the setting of simulation 3 produces outputs that take much longer than the others to homogenize, so that, at larger times, the output is much different from the output in the other settings. This feature should be introduced in the SE, in order to produce better predictions, but this is left for further research. Anyway, this prediction accuracy exercise highlights the subtle adjustments that are needed, when comparing predictions to actual data.

Since the SE is built up using all information in the shallow reservoir, we also performed an emulation study to investigate two aspects of the SE. First, we note that the whole simulated data for the estimation of the parameters of the SE (i.e., $\hat{\boldsymbol{\theta}}_j$ for $j = 1, \ldots, J$) might not, a priori, be necessary. Therefore, we also considered subsampling uniformly the simulator's outputs for given aspect ratios, density differences and time, i.e., the columns of $\mathbf{Y}_i$ in Figure 3. The subsamples represent respectively 60%, 30% and 10% of the simulated outcomes, on which the quantiles of interest are
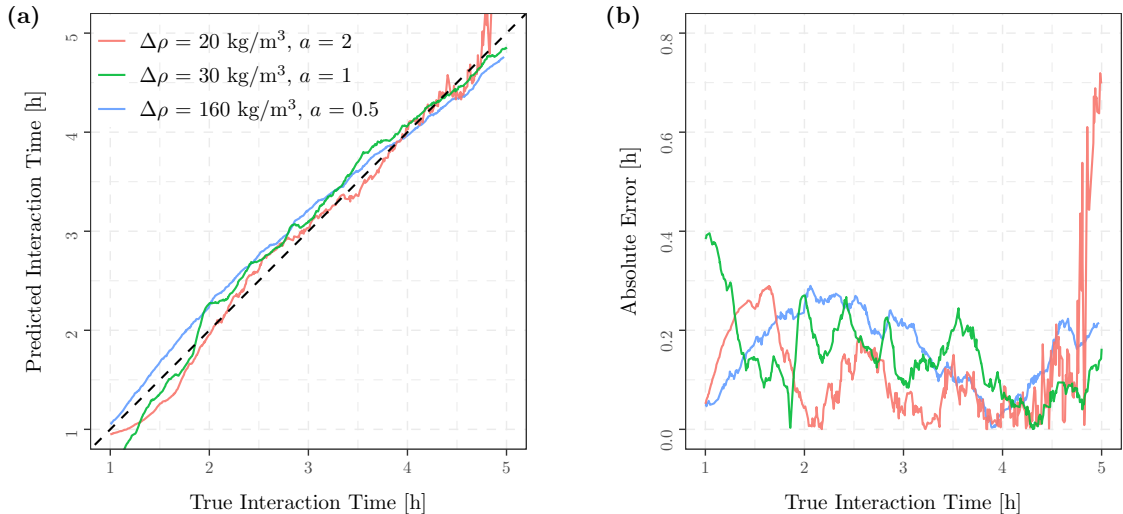
Figure 4. Panel (a): predicted (solid lines) versus true (dashed line) interaction times (in hours) across simulations 2-4 of Table 1, computed using (4). Panel (b): absolute prediction errors associated to each simulation setting.

then computed. Additionally, as an eruption could extract magma from progressively deeper portions of the magmatic reservoir, we emulated the accuracy of the SE in predicting the times considering the lower and upper half of the magma reservoir, separately. The predicted versus true interaction times (in hours) across simulations 2-4, computed using (4), are presented in Figure 5, for the different emulation settings. Panels (a)-(c) emulate the accuracy on the whole shallow reservoir, while panels (d)-(f) and panels (g)-(i) emulate the accuracy in respectively, the upper half and lower half parts of the shallow reservoir. Within each panel, the accuracy is assessed using different sampling proportions. In particular, panels (a)-(c) of Figure 5 show that, across the considered simulation settings, subsampling from the whole shallow reservoir does not significantly impact predictive accuracy. However, the remaining panels of Figure 5 highlight the presence of estimation biases even under a full sampling scheme. Such biases are more marked for simulation 4, reported in panels (c), (f) and (h), and they can be partially explained by the nature of this simulation. These biases can be generally associated to chamber stratification. Indeed, while the whole system is more or less going towards homogeneity, it does so in a way that the upper half shallow chamber contains more of one of the two end-member magmas, and the lower half shallow chamber contains more of the other. Having said that, it should be stressed that these biases are not due to an inaccurate adjustment of the SE, but instead constitute additional information for field data collection. For instance, if the available deposits from eruptions show a transition of chemistry from the bottom to the top of the deposit, then one would adapt the SE to separate the simulator outputs from the upper and lower half, so that better predictions can be built. In other words, when chemical gradients in erupted deposits can provide additional information on the modality of magma extraction from the subvolcanic reservoir, the SE can be adapted accordingly.

4. Error propagation

Obviously, in (4), the (fixed) parameters a, $\Delta\rho$ and $\hat{\mathbf{y}}$ are subject to measurement (or guessing) error, $\boldsymbol{f}(\cdot)$ is subject to approximation error, and the (fixed) parameters $\hat{\boldsymbol{\theta}}$ are subject to estimation error. The last two types of errors can be deduced from the properties of the estimators using model (2). We however found out that the approximation error
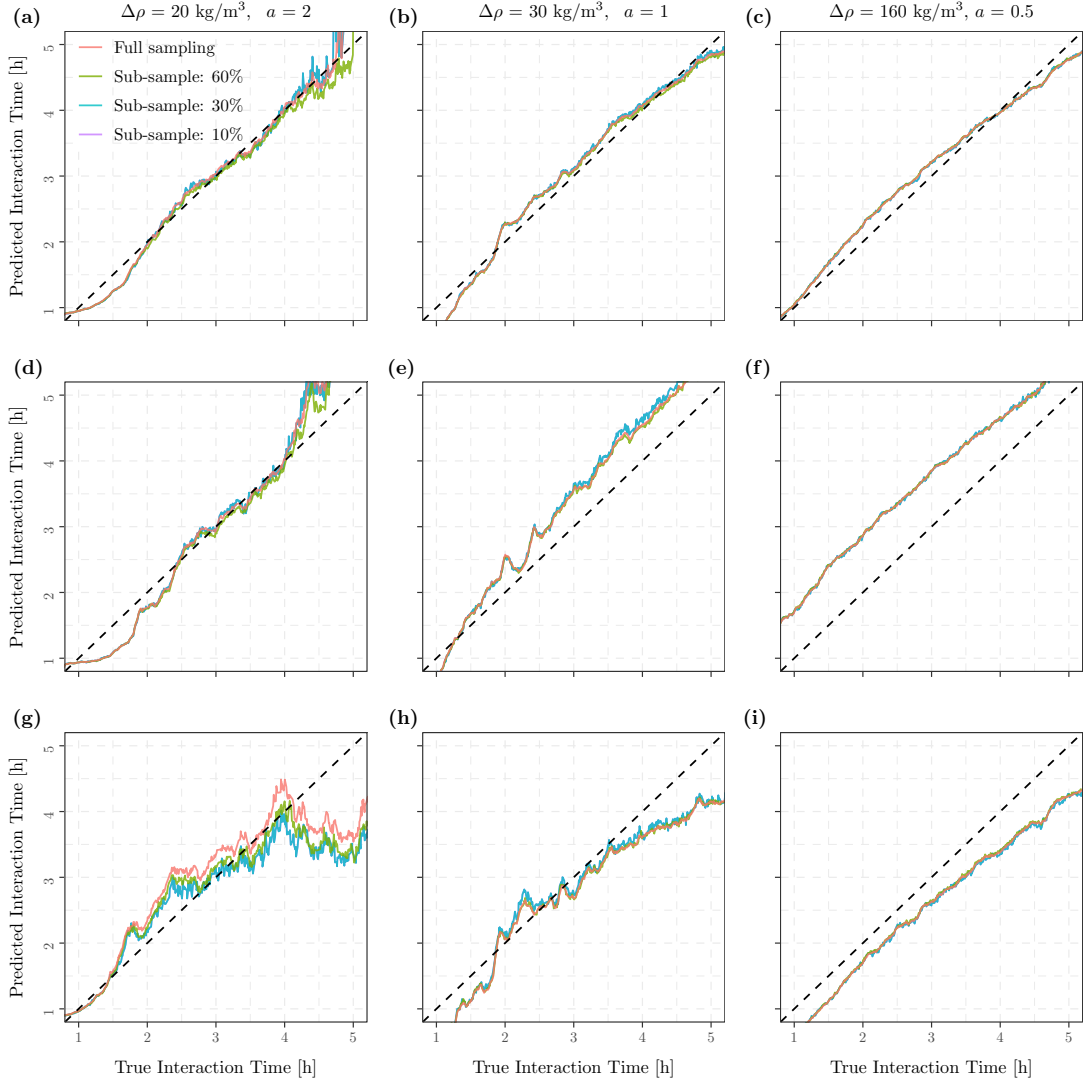
Figure 5. Predicted (solid lines) versus true (dashed lines) interaction times (in hours) across simulations 2-4 of Table 1, computed using (4). The predicted interactions times are computed on the whole shallow reservoir (panels (a)-(c)), the upper half part (panels (d)-(f)) and the lower half part (panels (g)-(i)) of the shallow reservoir. Within each panel, the predicted interactions times are computed on different (uniform) subsamples.

– due to the use of a statistical model $\boldsymbol{f}(\cdot)$ to approximate the true physical mechanism – is small (see Figure 4), and the estimation error for $\hat{\boldsymbol{\theta}}$ is negligible.

Measurement errors for a, $\Delta\rho$ and the elements of $\hat{\mathbf{y}}$ can be inferred from scientists' experience. All sources of error can then be included in the statistical emulation procedure to obtain a set of possible values for $\hat{t}$ in (4), from which confidence intervals can be built. This can be achieved through simulations. Indeed, one can consider that the errors are symmetrically distributed around the actual value of the parameters, so that, for each parameter, we can simulate an error drawn from a pre-specified distribution, such as the normal distribution. This is equivalent to simulate possible values for the different parameters, from a normal distribution, centered at the true value, with a pre-specified variance. For the latter, based on domain knowledge, a standard error of 10% of the actual value is usually expected. Let the elements $\hat{y}^*_{hj}$ of $\hat{\mathbf{y}}^*_h$, a^*_h and $\Delta\rho^*_h$, for $h = 1, \ldots, H$, be (independent) random realizations drawn from normal
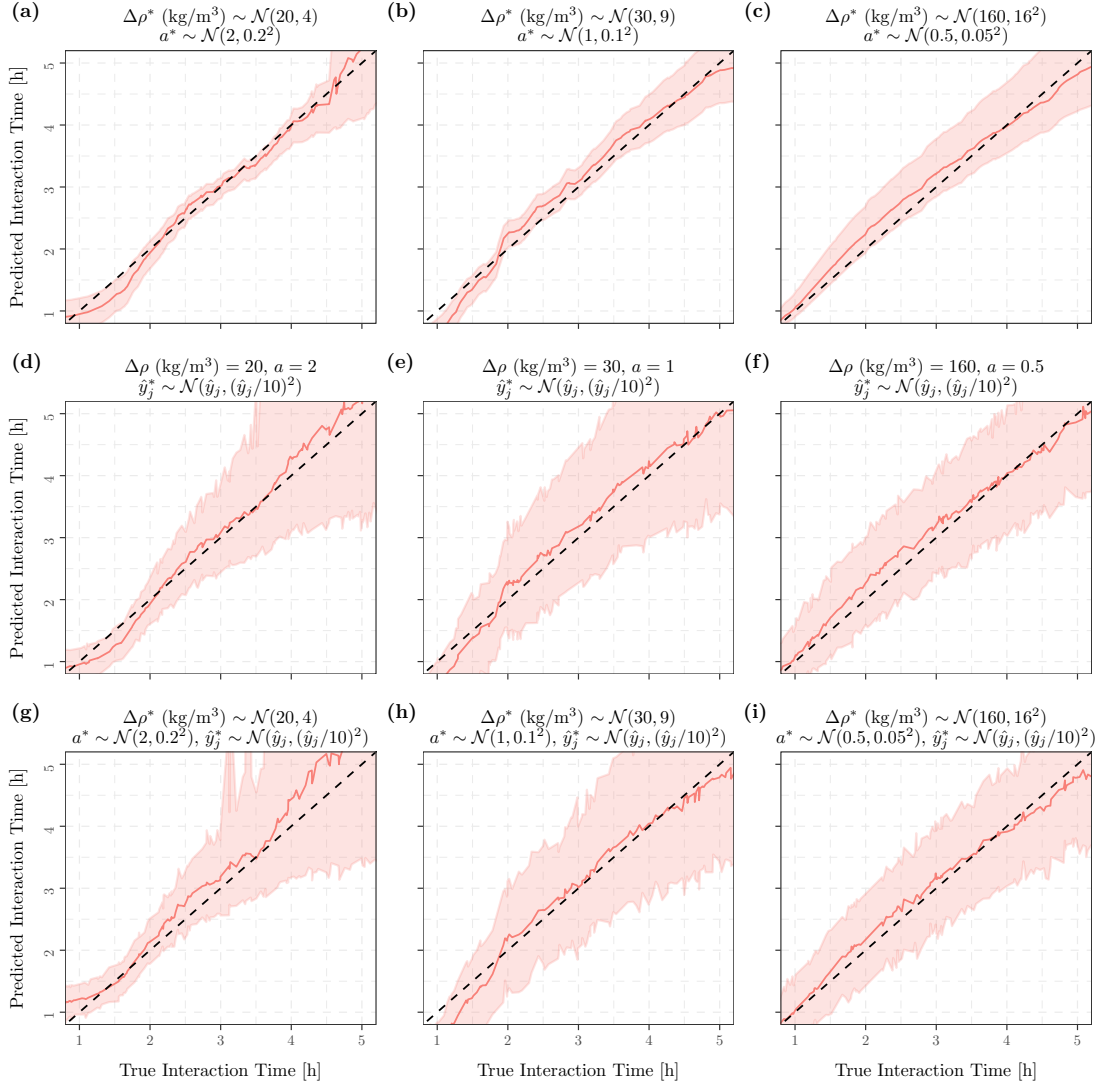
Figure 6. Sensitivity of the statistical emulator across simulations 2-4 of Table 1, where input parameters $\Delta\rho^*$ and a^* (panels (a)-(c)), $\hat{y}_j^*$ (panels (d)-(f)), $\Delta\rho^*$, a^*, and $\hat{y}_j^*$ (panels (g)-(i)) are drawn from normal distributions centered at their true values $(\Delta\rho, a, \hat{y}_j)$ with standard deviations equal to 10% of such true values. Average predicted (solid lines) versus true (dashed lines) interaction times (in hours), as well as 95% confidence intervals, are computed using $H = 200$ in (5). Each setting is restricted to a (uniform) subsample encompassing 25% of the locations sampled from the shallow reservoir.

distributions, then

$$\hat{t}_h^* = \arg\min_t \left(\hat{\mathbf{y}}_h^* - \hat{\boldsymbol{f}}(t, a_h^*, \Delta\rho_h^*, \hat{\boldsymbol{\theta}})\right)^T \hat{\boldsymbol{\Sigma}}(\hat{\boldsymbol{\theta}})^{-1} \left(\hat{\mathbf{y}}_h^* - \hat{\boldsymbol{f}}(t, a_h^*, \Delta\rho_h^*, \hat{\boldsymbol{\theta}})\right) \tag{5}$$

represents a suitable distribution for $\hat{t}$ that takes into account all (significant) sources of errors. Thus, a confidence interval at the $1 - \alpha$ confidence level for t is given by $(\hat{t}_{(l)}^*, \hat{t}_{(u)}^*)$, where $l = \lfloor (\alpha/2)H \rfloor$ and $u = \lceil (1 - \alpha/2)H \rceil$, with $x_{(i)}$ being the i-th order statistics, and with $\lfloor x \rfloor$, respectively $\lceil x \rceil$, being the integer smaller than or equal, respectively larger than or equal, to x.

Figure 6 presents 95% confidence intervals for predicted interaction times (in hours), across simulations 2-4 (from left to right), when some parameters are fixed and other are subject to random error. Specifically, in panels (a)-(c), both

a and $\Delta\rho$ are subject to random error while the elements of $\hat{\mathbf{y}}$ are fixed, in panels (d)-(f), a and $\Delta\rho$ are fixed while the elements of $\hat{\mathbf{y}}$ are subject to random error, and in panels (g)-(i) all parameters are subject to random error. Overall, predicted interaction times are close to the true ones across all simulation settings, and we note that the estimation variability increases as we assess for all input parameters (panels (g)-(i)). Confidence intervals are generally smaller than 20%, reaching up to 30%. Given the large uncertainties that characterize our understanding of inaccessible magmatic plumbing systems (Sigurdsson et al., 2015), these confidence intervals are rather narrow and allow us to provide meaningful estimates of pre-eruptive magmatic interaction times.

5. DISCUSSION

The results of our analysis show that the SE is capable of reproducing the results of the numerical model with small uncertainty when both the contrast in density and the shape of the reservoir in which the interaction between magma occurs are known (Figure 4). This is true also when we consider sub-samples of the simulated domain. Interestingly, for some of the simulations, differences emerge when considering the upper and lower half of the simulated domain (Figure 4 panels (e), (f), (h), (i)). This indicates that for the specific input parameters of these runs (Table 1), the interaction will generate a zoned magma reservoir with chemical differences between its lower and upper portions. This is of interest, as it shows under which range of input parameters of the model, the interaction between two magmas leads to chemical heterogeneities that can be identified in the deposits of the eruption (e.g., chemical difference along the stratigraphy of deposit).

The contrast in density between two magmas can be calculated from existing models providing magma density as a function of its chemistry and the pressure and temperature conditions at which the interaction was occurring (e.g., Lange 1997). The temperature and pressure at which the interaction occur can be estimated using thermobarometry (Nimis, Ulmer 1998; Neave, Putirka 2017; Jorgenson et al. 2022; Petrelli et al. 2020b). Clearly, temperature and pressure estimates, together with estimates of the volatile content of magmas, which impacts their density, are all associated with uncertainties. Additionally, the geometry of the reservoir could be defined using geophysics, but this would not be possible when studying past eruptions. Thus, to quantify the duration of the pre-eruptive interaction between magmas, and fundamentally, the associated uncertainty, it is essential to propagate all uncertainties associated with the input parameters of the model. This is when the advantages of statistical emulation become evident as the alternative would be to perform a large number of time consuming numerical simulations varying the input parameters within a range considered reasonable by the experts. The results of runs performed using the emulator and considering a normal distribution with 10% uncertainty for input parameters such as a and $\Delta\rho$ and the measurable parameters in $\hat{\mathbf{y}}$ (i.e. the distribution of chemistry of erupted magma), show that the uncertainty in the estimated interaction time preceding an eruption increases with the duration of interaction, but does not exceed 25-30% of the total interaction time (Figure 6).

As a byproduct, the SE provides insights on the sensitivity of model results to specific input parameters. Successive runs of the simulator must thus target specific regions of the parameters space that yield most representative results. Moreover, the emulator results obtained with large undersampling of the simulated outputs are practically indistinguishable from those obtained with the whole datasets (Figure 4). Eliminating unnecessary outputs would largely

decrease computational costs of large simulations, contributing to an overall leaner and more manageable workflow.

6. Conclusions

The Earth Sciences focus on phenomena that occurred in the past or at inaccessible depths, which inhibits our capacity to define with confidence the range of input parameters of numerical models targeting the quantification of geological processes. Additionally, because of the complexity of some physical models, the realisation of a large number of simulations, which would allow one to assess how uncertainty in the input parameter affects the final results, is prohibitive. Here, we use a specific application to volcanology that allows us to highlight the multiple advantages of combining physical modelling and statistical emulation. We show how to determine the duration of magma interaction preceding a volcanic eruption from the analysis of the distribution of the erupted rock chemistry. This particular case is appropriate for Campi Flegrei (Italy; Bagagli et al. 2017; Morgavi et al. 2017; Montagna et al. 2022). The approach we present here could be applied to past eruptions of Campi Flegrei to determine the duration of the period of unrest preceding any volcanic eruption throughout its eruptive history. The approach consists in measuring the distribution of chemical composition of the rocks released by a volcanic eruption and in its comparison with the results of a SE calibrated on the base of physical models realised over a wide range of conditions and duration.

The results of our analysis show that statistical emulation provides an excellent mean to quantify the uncertainty in duration of magma interaction preceding a volcanic eruption from the distribution of chemical composition of the erupted rocks.

7. Bibliography

Annen C, Blundy J D, Sparks R S J. The genesis of intermediate and silicic magmas in deep crustal hot zones // Journal of Petrology. 2006. 47, 3. 505–539.

Arienzo I., Civetta L., Heumann A., Wörner G., Orsi G. Isotopic evidence for open system processes within the Campanian Ignimbrite (Campi Flegrei - Italy) magma chamber // Bulletin of Volcanology. 2009. 71, 3. 285–300.

Arienzo I, Moretti R, Civetta L, Orsi G, Papale P. The feeding system of Agnano - Monte Spina eruption (Campi Flegrei, Italy): Dragging the past into present activity and future scenarios // Chemical Geology. 2010. 270, 1-4. 135–147.

Bagagli M., Montagna C P, Papale P., Longo A. Signature of magmatic processes in strainmeter records at Campi Flegrei (Italy) // Geophys. Res. Lett. jan 2017. 44, 2. 718–725.

Blundy J, Cashman K. Ascent-driven crystallisation of dacite magmas at Mount St Helens, 1980-1986 // Contribution to mineralogy and petrology. 2001. 140, 6. 631–650.

Blundy J D, Sparks R S J. Petrogenesis of Mafic Inclusions in Granitoids of the Adamello Massif, Italy // Journal of Petrology. jan 1992. 33, 5. 1039–1104.

Bohrson Wendy A., Spera Frank J, Ghiorso Mark S, Brown Guy A, Creamer Jeffrey B, Mayfield Aaron. Thermodynamic Model for Energy-Constrained Open-System Evolution of Crustal Magma Bodies Undergoing Simultaneous Recharge, Assimilation and Crystallization: the Magma Chamber Simulator // Journal of Petrology. 2014. 55, 9. 1685–1717.

Caricchi Luca, Sheldrake Tom E., Blundy Jonathan D. Modulation of magmatic processes by CO_2 flushing // Earth Planet. Sci. Lett. 2018. 491. 160–171.

Caricchi Luca, Simpson Guy, Schaltegger Urs. Zircons reveal magma fluxes in the Earth's crust // Nature. 2014. 511, 7510. 457–461.

Caricchi Luca, Townsend Meredith, Rivalta Eleonora, Namiki Atsuko. The build-up and triggers of volcanic eruptions // Nature Reviews Earth & Environment. 2021. 2, 7. 458–476.

Cashman K V, Marsh B D. Crystal size distribution (CSD) in rocks and the kinetics and dynamics of crystallization II: Makaopuhi lava lake // Contribution to mineralogy and petrology. 1988. 99, 3. 292–305.

Cassidy Mike, Castro Jonathan M, Helo Christoph, Troll Valentin R, Deegan Frances M, Muir Duncan, Neave David A, Mueller Sebastian P. Volatile dilution during magma injections and implications for volcano explosivity // Geology. 2016. 44, 12. 1027–1030.

Chandrasekhar S. Hydrodynamic and Hydromagnetic Stability. 2013. 704.

Chiodini G., Caliro S., De Martino P., Avino R., Gherardi F. Early signals of new volcanic unrest at Campi Flegrei caldera? Insights from geochemical data and physical simulations // Geology. 2012. 40, 10. 943–946.

Cooper Kari M, Kent Adam J R. Rapid remobilization of magmatic crystals kept in cold storage // Nature. 2014. 1–18.

Currin C., Mitchell T., Morris M., Ylvisaker D. Bayesian prediction of deterministic functions, with applications to the design and analysis of computer experiments // Journal of the American Statistical Association. 1991. 86. 953–963.

Davidson J P, Morgan D J, Charlier B L A, Harlou R, Hora J M. Microsampling and Isotopic Analysis of Igneous Rocks: Implications for the Study of Magmatic Systems // Annual Review of Earth and Planetary Sciences. 2007. 35, 1. 273–311.

Di Renzo V., Arienzo I., Civetta L., D'Antonio M., Tonarini S., Di Vito M. A., Orsi G. The magmatic feeding system of the Campi Flegrei caldera: Architecture and temporal evolution // Chemical Geology. 2011. 281, 3-4. 227–241.

Druitt T. H., Costa Fidel, Deloule E., Dungan M., Scaillet B. Decadal to monthly timescales of magma transfer and reservoir growth at a caldera volcano // Nature. 2012. 482, 7383. 77–80.

Edmonds M, Aiuppa A, Humphreys M, Moretti R, Giudice G, Martin R S, Herd R A, Christopher T. Excess volatiles supplied by mingling of mafic magma at an andesite arc volcano // Geochemistry Geophysics Geosystems. 2010. 11.

Edmonds Marie, Cashman Katharine V, Holness Marian, Jackson Matthew. Architecture and dynamics of magma reservoirs // Phil. Trans. R. Soc. Lond. A. 2019. 377. 20180298.

Forni Francesca, Degruyter W, Bachmann O, De Astis G, Mollo S. Long-term magmatic evolution reveals the beginning of a new caldera cycle at Campi Flegrei // Science Advances. nov 2018. 4. 1–12.

Fourmentraux Céline, Métrich Nicole, Bertagnini Antonella, Rosi Mauro. Crystal fractionation, magma step ascent, and syn-eruptive mingling: The Averno 2 eruption (Phlegraean Fields, Italy) // Contributions to Mineralogy and Petrology. 2012. 163, 6. 1121–1137.

Garg Deepak, Longo Antonella, Papale Paolo. Computation of compressible and incompressible flows with a space–time stabilized finite element method // Computers & Mathematics with Applications. 2018a. 75, 12. 4272–4285.

Garg Deepak, Longo Antonella, Papale Paolo. Modeling Free Surface Flows Using Stabilized Finite Element Method // Mathematical Problems in Engineering. 2018b. 2018. 1–9.

Garg Deepak, Papale Paolo. High-performance computing of 3D magma dynamics, and comparison with 2D simulation results // Frontiers in Earth Science. 2022.

Garg Deepak, Papale Paolo, Colucci Simone, Longo Antonella. Long-lived compositional heterogeneities in magma chambers, and implications for volcanic hazard // Scientific Reports. 2019. 9, 1. 3321.

Giordano D, Russell JK, Dingwell DB. Viscosity of magmatic liquids: A model // Earth Planet. Sc. Lett. 2008. 271. 123–134.

Glazner A F, Bartley J M, Coleman D S, Gray W, Taylor R Z. Are plutons assembled over millions of years by amalgamation from small magma chambers? // GSA TODAY. jan 2004. 14. 4–11.

Gualda Guilherme A R, Ghiorso Mark S, Lemons Robin V, Carley Tamara L. Rhyolite-MELTS: a Modified Calibration of MELTS Optimized for Silica-rich, Fluid-bearing Magmatic Systems // Journal of Petrology. 2012. 53, 5. 875–890.

Guillas S., Sarri A., Day S. J., Liu X., Dias F. Functional emulation of high resolution tsunami modelling over Cascadia // Annals of Applied Statistics. 2018. 12. 2023–2053.

Heap Michael J, Villeneuve Marléne, Albino Fabien, Farquharson Jamie I, Brothelande Elodie, Amelung Falk, Got Jean-Luc, Baud Patrick. Towards more realistic values of elastic moduli for volcano modelling // J. Volcanol. Geotherm. Res. 2020. 390. 106684.

Hess K U, Dingwell D B. Viscosities of hydrous leucogranitic melts: A non-Arrhenian model // American Mineralogist. 1996. 81. 1297–1300.

Higdon D., Gattiker J., Williams B., Rightley M. Computer model calibration using high-dimensional output // Journal of the American Statistical Association. 2008. 103. 570–583.

Higgins M D. Measurement of crystal size distributions // American Mineralogist. 2000. 85, 9. 1105–1116.

Humphreys M C S, Edmonds M, Plail M, Barclay J, Parkes D, Christopher T. A new method to quantify the real supply of mafic components to a hybrid andesite // Contribution to mineralogy and petrology. 2012. 165, 1. 191–215.

Iovine Raffaella Silvia, Fedele Lorenzo, Mazzeo Fabio Carmine, Arienzo Ilenia, Cavallo Andrea, Wörner Gerhard, Orsi Giovanni, Civetta Lucia, D'Antonio Massimo. Timescales of magmatic processes prior to the ∼4.7 ka Agnano-Monte Spina eruption (Campi Flegrei caldera, Southern Italy) based on diffusion chronometry from sanidine phenocrysts // Bull. Volcanol. 2017. 79, 2.

Ishii M, Zuber N. Drag coefficient and relative velocity in bubbly, droplet or particulate flows // AiChE J. 1979. 25. 843–855.

Jackson M D, Blundy J, Sparks R S J. Chemical differentiation, cold storage and remobilization of magma in the Earth's crust // Nature. 2018.

Jorgenson C., Higgins O., Petrelli M., Bégué F., Caricchi L. A Machine Learning-Based Approach to Clinopyroxene Thermobarometry: Model Optimization and Distribution for Use in Earth Sciences // Journal of Geophysical Research: Solid Earth. 2022.

Karakas Ozge, Degruyter Wim, Bachmann Olivier, Dufek Josef. Lifetime and size of shallow magma bodies controlled by crustal-scale magmatism // Nature Geoscience. 2017. 310. 511.

Keller Tobias, Suckale Jenny. A continuum model of multi-phase reactive transport in igneous systems // Geophysical Journal International. oct 2019. 219, 1. 185–222.

Kennedy M. C., O'Hagan A. Bayesian calibration of computermodels // Journal of the Royal Statistical Society: Series B (Statistical Methodology). 2001. 63. 425–464.

La Spina Giuseppe, Arzilli Fabio, Burton Mike R., Polacci Margherita, Clarke Amanda B. Role of volatiles in highly explosive basaltic eruptions // Communications Earth & Environment. XII 2022. 3, 1. 156.

Lange R A. A revised model for the density and thermal expansivity of K 2 O-Na 2 O-CaO-MgO-Al 2 O 3-SiO 2 liquids from 700 to 1900 K: extension to crustal magmatic temperatures // Contribution to mineralogy and petrology. 1997. 130, 1. 1–11.

Lavallée Yan, Hess Kai-Uwe, Cordonnier Benoit, Bruce Dingwell Donald. Non-Newtonian rheological law for highly crystalline dome lavas // Geology. 2007. 35, 9. 843.

Lejeune A M, Richet P. Rheology of Crystal-Bearing Silicate Melts - an Experimental-Study at High Viscosities // Journal of Geophysical Research-Solid Earth. 1995. 100. 4215–4229.

Longo A, Barsanti M, Cassioli A, Papale P. A finite element Galerkin/least-squares method for computation of multicomponent compressible–incompressible flows // Comput. Fluids. 2012a. 67. 57–71.

Longo Antonella, Papale Paolo, Vassalli Melissa, Saccorotti Gilberto, Montagna Chiara P, Cassioli Andrea, Giudice Salvatore, Boschi Enzo. Magma convection and mixing dynamics as a source of Ultra-Long-Period oscillations // Bulletin of Volcanology. 2012b. 74, 4. 873–880.

Maclennan J. Mafic tiers and transient mushes: evidence from Iceland // Philosophical Transactions of the Royal Society A: Mathematical, Physical and Engineering Sciences. 2019. 377, 2139. 20180021.

Mahmood A., Wolpert R. L., Pitman E. B. A Physics-Based Emulator for the Simulation of Geophysical Mass Flows // Uncertainty Quantification. 2015. 3. 562–585.

Mangiacapra A., Moretti R., Rutherford M., Civetta L., Orsi G., Papale P. The deep magmatic system of the Campi Flegrei caldera (Italy) // Geophysical Research Letters. 2008. 35, 21. L21304.

Marsh B D. On the Crystallinity, Probability of Occurrence, and Rheology of Lava and Magma // Contribution to mineralogy and petrology. 1981. 78, 1. 85–98.

Matoza Robin S., Roman Diana C. One hundred years of advances in volcano seismology and acoustics // Bulletin of Volcanology. VIII 2022. 84, 9. 86.

Mogi K. Relations between the Eruptions of Various Volcanoes and the Deformations of the Ground Surfaces around them // B. Earthq. Res. I. Tokyo. 1958. 36. 99–134.

Montagna CP, Papale P. Time scales of shallow magma chamber replenishment at Campi Flegrei caldera. 2018. EarthArXiv https://osf.io/bze9w.

Montagna CP, Papale P, Longo A. Timescales of mingling in shallow magmatic reservoirs // Geological Society, London, Special Publications. 2015. 422. SP422–6.

Montagna Chiara P., Papale Paolo, Longo Antonella. Magma Chamber Dynamics at the Campi Flegrei Caldera, Italy // Campi Flegrei. Berlin, Heidelberg: Springer Berlin Heidelberg, 2022. 201–217. Series Title: Active Volcanoes of the World.

Morgavi Daniele, Arienzo Ilenia, Montagna Chiara Paola, Perugini Diego, Dingwell Donald B. Magma Mixing: History and Dynamics of an Eruption Trigger // Volcanic Unrest. 2017. 123–137.

Morgavi Daniele, Arzilli Fabio, Pritchard Chad, Perugini Diego, Mancini Lucia, Larson Peter, Dingwell Donald B. The Grizzly Lake complex (Yellowstone Volcano, USA): Mixing between basalt and rhyolite unraveled by microanalysis and X-ray microtomography // Lithos. sep 2016. 260. 457–474.

Neave D A, Maclennan J, Hartley M E, Edmonds M, Thordarson T. Crystal Storage and Transfer in Basaltic Systems: the Skuggafjoll Eruption, Iceland // Journal of Petrology. 2014.

Neave David A., Putirka Keith D. A new clinopyroxene-liquid barometer, and implications for magma storage pressures under Icelandic rift zones // American Mineralogist. 2017. 102, 4. 777–794.

Newey Whitney K, McFadden Daniel. Large sample estimation and hypothesis testing // Handbook of econometrics. 1994. 4. 2111–2245.

Nimis P. A Clinopyroxene Geobarometer for Basaltic Systems Based on Crystal-Structure Modeling // Contribution to mineralogy and petrology. 1995.

Nimis P, Ulmer P. Clinopyroxene geobarometry of magmatic rocks Part 1: An expanded structural geobarometer for anhydrous and hydrous, basic and ultrabasic systems // Contribution to mineralogy and petrology. 1998. 133, 1-2. 122–135.

Papale P., Montagna C P, Longo A. Pressure evolution in shallow magma chambers upon buoyancy-driven replenishment // Geochemistry, Geophys. Geosystems. 2017. 18.

Papale P, Moretti R, Barbato D. The compositional dependence of the saturation surface of H_2O+CO_2 fluids in silicate melts // Chem. Geol. 2006. 229, 1-3. 78–95.

Perugini D, Poli G. Viscous fingering during replenishment of felsic magma chambers by continuous inputs of mafic magmas: Field evidence and fluid-mechanics experiments // Geology. jan 2005. 33, 1. 5–8.

Perugini Diego, De Campos Cristina P, Petrelli Maurizio, Dingwell Donald B. Concentration variance decay during magma mixing: a volcanic chronometer // Scientific Reports. 2015.

Petrelli M., Caricchi L., Perugini D. Machine Learning Thermo-Barometry: Application to Clinopyroxene-Bearing Magmas // Journal of Geophysical Research: Solid Earth. 2020a.

Petrelli M., Caricchi L., Perugini D. Machine Learning Thermo-Barometry: Application to Clinopyroxene-Bearing Magmas // Journal of Geophysical Research: Solid Earth. 2020b. 125, 9.

Petrone Chiara Maria, Braschi Eleonora, Francalanci Lorella, Casalini Martina, Tommasini Simone. Rapid mixing and short storage timescale in the magma dynamics of a steady-state volcano // Earth Planet. Sci. Lett. 2018. 492. 206–221.

Pistone Mattia, Caricchi Luca, Ulmer Peter, Burlini Luigi, Ardia Paola, Reusser Eric, Marone Federica, Arbaret Laurent. Deformation experiments of bubble- and crystal-bearing magmas: Rheological and microstructural analysis // Journal of Geophysical Research. 2012. 117, B5. B05208.

Poland Michael P., Dalfsen Elske de Zeeuw-van. Volcano geodesy: A critical tool for assessing the state of volcanoes and their potential for hazardous eruptive activity // Forecasting and Planning for Volcanic Hazards, Risks, and Disasters. 2021. 75–115.

Putirka K D. Thermometers and Barometers for Volcanic Systems // Reviews in Mineralogy and Geochemistry. 2008a. 69, 1. 61–120.

Putirka Keith D. Thermometers and Barometers for Volcanic Systems // Reviews in Mineralogy and Geochemistry. 2008b.

Reid R C, Prausnitz J, Sherwood T. The properties of gases and liquids. New York: McGraw Hill, 1977. 3rd. (International Series in the Physical and Chemical Engineering Sciences).

Ridolfi F, Renzulli A, Perugini D, Cesare B, Braga R. Unravelling the complex interaction between mantle and crustal magmas encoded in the lavas of San Vincenzo (Tuscany, Italy). Part II: Geochemical overview and ... // LITHOS. 2015.

Rummel Lisa, Kaus Boris J P, Baumann Tobias S., White Richard W., Riel Nicolas. Insights into the Compositional Evolution of Crustal Magmatic Systems from Coupled Petrological-Geodynamical Models // Journal of Petrology. oct 2020. 61, 2.

Sacks J., Welch W. J., Mitchell T. J., Wynn H. P. Design and analysis of computer experiments // Statistical Science. 1989. 409–423.

Salter J. M., Williamson D. A comparison of statistical emulation methodologies for multi-wave calibration of environmental models // Environmetrics. 2016. 27. 507–523.

Santner T. J., Williams B. J., Notz W. The design and analysis of computer experiments. Berlin: Springer Science & Business Media, 2003.

Selva Jacopo, Marzocchi Warner, Papale P., Sandri Laura. Operational eruption forecasting at high-risk volcanoes: the case of Campi Flegrei, Naples // Journal of Applied Volcanology. 2012. 1. 5.

Sigurdsson Haraldur, Houghton Bruce, McNutt Stephen R., Rymer Hazel, Stix John. The Encyclopedia of Volcanoes. 2015.

Stock Michael J., Humphreys Madeleine C.S., Smith Victoria C., Isaia Roberto, Brooker Richard A., Pyle . Tracking volatile behaviour in sub-volcanic plumbing systems using apatite and glass: Insights into pre-eruptive processes at Campi Flegrei, Italy // Journal of Petrology. 2018. 59, 12. 2463–2492.

Tonarini Sonia, D'Antonio Massimo, Di Vito Mauro Antonio, Orsi Giovanni, Carandente Antonio. Geochemical and B–Sr–Nd isotopic evidence for mingling and mixing processes in the magmatic system that fed the Astroni volcano (4.1–3.8 ka) within the Campi Flegrei caldera (southern Italy) // Lithos. 2009. 107, 3-4. 135–151.

Wark D.A., Hildreth W., Spear F.S., Cherniak D.J., Watson E.B. Pre-eruption recharge of the Bishop magma system // Geology. 2007. 35, 3. 235.

Wei Zihan, Qin Zhipeng, Suckale Jenny. Magma Mixing During Conduit Flow is Reflected in Melt-Inclusion Data From Persistently Degassing Volcanoes // Journal of Geophysical Research: Solid Earth. 2022. 127, 2. e2021JB022799. e2021JB022799 2021JB022799.

Yang Q., Pitman E. B., Spiller E., Bursik M., Bevilacqua A. Novel statistical emulator construction for volcanic ash transport model Ash3d with physically motivated measures // Proceedings of the Royal Society A. 2020. 476. 20200161.

Zellmer Georg F, Iizuka Yoshiyuki, Lormand Charline, Moebis Anja. Beyond crystal mushes: evidence for uptake of high-T pyroxene antecrysts from mid- to upper crustal andesites into tephras from the Central Plateau, New Zealand // New Zealand Journal of Geology and Geophysics. 2020. 0, 0. 1–13.

Zhong Xin, Dabrowski Marcin, Jamtveit Bjorn. Analytical solution for the stress field in elastic half-space with a spherical pressurized cavity or inclusion containing eigenstrain // Geophysical Journal International. II 2019. 216, 2. 1100–1115.